Research Article
Aquatic Functional Products

Eco-Friendly Chitosan–Silica Composite Coatings Derived from Crab Shell Waste for Enhanced Corrosion Protection of ASTM A36 Steel

Wardah Maulida Saldi, Erna Hastuti

[The author informations are in the declarations section. This article is published by ETFLIN in Aquatic Functional Products, Volume 1, Issue 1, 2025, Page 1-8. DOI 10.58920/etflin000000 (pending update; Crossmark will be active once finalized)]

Received: 29 September 2025
Revised: 16 December 2025
Accepted: 21 December 2025
Published: 25 December 2025

Editor: Ramanda Ahmad Rizal Rifa'i

Keywords: Chitosan, Silica, Composite coating, ASTM A36 steel, Corrosion resistance.

Abstract: Corrosion of carbon steel in chloride-rich environments remains a critical challenge, while conventional chitosan-based coatings often suffer from limited barrier integrity and durability. This study addresses this limitation by developing an eco-friendly chitosan–silica composite coating derived from crab shell waste and systematically evaluating the effect of silica loading (1–4%) on the corrosion protection of ASTM A36 steel under 10% NaCl immersion. Chemical interactions were examined using Fourier-transform infrared spectroscopy (FTIR), while corrosion performance was assessed through weight loss measurements, electrochemical impedance spectroscopy (EIS), and surface morphology observations. FTIR results confirmed the successful incorporation of silica and enhanced hydrogen bonding between silanol groups and chitosan chains. The composite coating containing 2% silica exhibited the highest corrosion resistance, achieving the lowest corrosion rate and the highest polarization resistance compared to pure chitosan and uncoated steel. The improved performance is attributed to enhanced barrier properties of the chitosan–silica composite, where the presence of well-dispersed silica particles limits chloride ion penetration. At higher silica loadings, corrosion protection declined, likely due to reduced coating uniformity. These findings demonstrate that controlled silica reinforcement introduces a distinct corrosion protection mechanism beyond conventional chitosan coatings and highlight the potential of bio-based hybrid coatings for sustainable steel protection.

Introduction

Corrosion is one of the most persistent degradation mechanisms affecting metallic materials, particularly carbon steels used in industrial environments (1). Low-carbon steel ASTM A36 is widely applied in construction, pipelines, shipbuilding, and water infrastructure because of its low cost and adequate mechanical properties (2). Despite these advantages, its direct exposure to aqueous and chloride-containing environments makes it highly vulnerable to electrochemical corrosion processes (3, 4). The economic impact of corrosion is significant, accounting for approximately 3–4% of global GDP each year (5). In addition to financial losses, corrosion poses serious safety risks, accelerates material failure, and contributes to environmental degradation (6).

Conventional corrosion protection strategies include metallic coatings, cathodic protection, and the use of organic or inorganic inhibitors. Although effective, these methods often suffer from high implementation costs, environmental concerns, limited service life, or operational complexity (7). As a result, increasing attention has been directed toward sustainable and environmentally friendly alternatives. Among them, biopolymer-based coatings have emerged as promising corrosion inhibitors due to their low toxicity and renewability (8).

Chitosan, a deacetylated derivative of chitin obtained from crustacean shell waste, has attracted particular interest because of its biodegradability, film-forming ability, and strong affinity for metal surfaces through amino and hydroxyl functional groups (9). These characteristics allow chitosan to adsorb onto steel surfaces and act as a physical barrier against corrosive species. However, pure chitosan coatings often exhibit limited mechanical strength and reduced stability in acidic or high-salinity environments, which restricts their long-term protective performance.

Recent studies have demonstrated that chitosan-based coatings can effectively reduce the corrosion rate of carbon steel in aqueous and chloride-containing environments due to their film-forming ability and strong interaction with metal surfaces (10). Furthermore, several studies on biopolymer–silica composite coatings have reported improved barrier properties and mechanical stability compared to pure biopolymer coatings (11). However, most

of these studies focus on a single filler content or short-term exposure, and do not systematically evaluate the effect of silica loading on the electrochemical behavior of carbon steel under high-chloride conditions.

To overcome these limitations, the incorporation of inorganic fillers such as silica has been proposed. Silica particles can improve coating compactness by filling microvoids within the polymer matrix, thereby reducing permeability to water and chloride ions. In addition, the interaction between silanol groups and chitosan chains can enhance interfacial adhesion and mechanical stability, leading to improved barrier performance under aggressive conditions (12). Despite these advantages, the influence of silica content on the electrochemical behavior of chitosan-based coatings has not been systematically investigated, particularly for industrial-grade carbon steels in chloride-rich media.

In this study, a chitosan–silica composite coating derived from crab shell waste is developed as an eco-friendly and cost-effective protective layer for ASTM A36 steel. To the best of our knowledge, no prior studies have systematically correlated silica loading levels (1–4%) with the resulting electrochemical impedance response and degradation behavior of chitosan-based coatings under prolonged immersion in 10% NaCl solution. The coatings were applied using a simple brush method with varying silica concentrations and evaluated using Fourier-transform infrared spectroscopy (FTIR), weight loss measurements, and electrochemical impedance spectroscopy (EIS). This work provides new insights into the structure–property relationship of bio-based hybrid coatings and highlights their potential for sustainable corrosion protection in industrial environments.

Methodology

Study Design

This study employed an experimental design to evaluate the effectiveness of crab-shell-derived chitosan reinforced with silica as a protective coating for ASTM A36 steel against corrosion. The objective was to develop a sustainable bio-based hybrid coating with enhanced physicochemical stability and anticorrosion performance in chloride-rich environments. Comparative analyses were conducted between uncoated steel, steel coated with pure chitosan, and steel coated with chitosan–silica composites containing varying silica loadings (1–4% w/w).

Materials and Reagents

Crab shells were collected as seafood waste from local restaurants and processed to obtain chitosan. ASTM A36 steel specimens were cut into square coupons (20 × 20 × 2 mm). Before coating, all specimens were mechanically prepared to ensure surface cleanliness and reproducibility. Analytical-grade reagents included sodium hydroxide (NaOH), hydrochloric acid (HCl), acetic acid (CH_3COOH), and sodium chloride (NaCl). Commercial silica powder (SiO_2, ≥99% purity) with a micron-scale particle size was used as the inorganic filler. Deionized water (resistivity ≥18.2 MΩ·cm) was used for all solution preparations.

Surface Preparation of ASTM A36 Steel

Before coating application, ASTM A36 steel specimens were mechanically abraded using silicon carbide (SiC) abrasive papers to remove surface contaminants and loosely adherent oxides. The samples were then degreased, rinsed thoroughly with deionized water, and dried at room temperature. This surface preparation procedure was performed to ensure adequate coating adhesion and reproducible corrosion testing conditions, following general recommendations for corrosion studies.

Preparation of Chitosan

Chitosan was extracted from crab shell powder (200 mesh) through sequential deproteinization, demineralization, and deacetylation. Deproteinization was conducted by treating 50 g of crab shell powder with 500 mL of NaOH solution (3.5% w/v) under microwave irradiation at 100 W for 15 min, followed by filtration and rinsing until neutral pH was reached. Demineralization was achieved by stirring the residue with 750 mL of HCl solution (1 N) for 60 min. The resulting chitin was washed and dried prior to deacetylation, which was carried out using NaOH (40% w/v) at a chitin-to-solution ratio of 1:20 (b/v) under microwave irradiation at 1200 W for 40 min. The obtained chitosan was neutralized, dried, and ground for further use.

Preparation of Chitosan–Silica Composite Coatings

Five coating systems were prepared: uncoated ASTM A36 steel (blank), steel coated with pure chitosan, and steel coated with chitosan–silica composites containing 1%, 2%, 3%, and 4% silica by weight. To prepare the coating solution, 5 g of chitosan was dissolved in 100 mL of acetic acid solution (2% v/v) under continuous magnetic stirring for 3 h at room temperature until a homogeneous solution was obtained. Silica powder was then added according to the desired loading and stirred until uniform dispersion was achieved.

The coating suspensions were applied to the steel substrates using a manual brush technique. To minimize variability and ensure coating uniformity, each specimen was coated using the same number of brush strokes applied in a single direction. The coated specimens were dried at room temperature (25 ± 2 °C) for 24 h under ambient laboratory conditions before corrosion testing and subsequently stored in a desiccator to prevent premature moisture absorption.

The average coating thickness was measured using a digital micrometer at multiple locations on each specimen, and the reported values represent the mean thickness of the coating layer.

Corrosion Testing

Corrosion resistance was evaluated using a 10% NaCl aqueous solution as the corrosive medium. Coated and uncoated steel specimens were immersed in 200 mL of NaCl solution for 7 days at ambient temperature. After immersion, corrosion products were removed, and weight loss measurements were conducted in accordance with ASTM G31-72. The corrosion rate (CR, $mm \cdot y^{-1}$) was calculated using **Equation 1.**

$$CR = \frac{K \cdot \Delta W}{A \cdot t \cdot \rho}$$

Equation 1 | CR = Corrosion rate ($mm \cdot y^{-1}$), K = Conversion constant (87.6), ΔW = Weight loss (mg), A = Exposed surface area (cm^2), t = Immersion time (h), ρ = Density of steel (7.85 $g \cdot cm^{-3}$).

Spectroscopic and Electrochemical Characterization

Fourier-transform infrared spectroscopy (FTIR, 4000–400 cm^{-1}, Bruker Tensor series) was employed to identify functional groups present in chitosan and chitosan–silica composite coatings. Electrochemical impedance spectroscopy (EIS) measurements were performed using a conventional three-electrode cell configuration, with the coated steel as the working electrode, a saturated calomel electrode as the reference electrode, and a platinum counter electrode. Impedance spectra were recorded over a frequency range of 10^{-2} to 10^{5} Hz using a 10 mV AC perturbation.

The EIS data were analyzed using equivalent circuit modeling consisting of solution resistance (Rs), polarization resistance (Rp), and a constant phase element (CPE). The fitting quality was evaluated based on chi-square (χ^2) values and relative fitting errors below 10%.

Data Analysis

All corrosion rate and EIS measurements were performed in triplicate. Statistical analysis was conducted using one-way analysis of variance (ANOVA), followed by Tukey's post-hoc test at a significance level of $\alpha = 0.05$. FTIR spectra were analyzed qualitatively by peak assignment, while EIS fitting was performed using ZView software.

Ethical Considerations

This study did not involve human participants or vertebrate animals. Crab shell waste was obtained from food industry by-products; therefore, ethical approval was not required.

Results

Coating Characterization by FTIR Spectroscopy

Chitosan was successfully extracted from crab shell waste through sequential deproteinization, demineralization, and deacetylation processes, yielding 237 g of chitosan from 500 g of dried shell material, as summarized in **Table 1**.

Table 1. Yield of chitosan production.

Process	Powder Weight (g)
Crab shell (raw)	500
After deproteinization	421
After demineralization	398
After deacetylation	237

Table 2. Coating variations and sample codes.

Code	Coating Composition
BB	Uncoated (Blank)
BK	Chitosan
BKS1	Chitosan + 1% Silica
BKS2	Chitosan + 2% Silica
BKS3	Chitosan + 3% Silica
BKS4	Chitosan + 4% Silica

The resulting chitosan was subsequently dissolved in acetic acid and combined with silica at different loadings to prepare composite coating formulations. The coating compositions and sample codes are listed in **Table 2**.

Fourier-transform infrared (FTIR) spectroscopy was employed to examine the chemical structure of chitosan and its interaction with silica in the composite coatings. High-resolution FTIR spectra were recorded for pure chitosan (BK) and chitosan–silica composites with different silica loadings (BKS1–BKS4). Representative spectra are shown in **Figure 1**, while key absorption bands are summarized in **Table 3**.

The FTIR spectrum of pure chitosan (BK) exhibits a broad absorption band in the range of 3000–3500 cm^{-1}, attributed to overlapping O–H and N–H stretching vibrations, indicating extensive hydrogen bonding within the chitosan matrix. Characteristic absorption bands at approximately 1637 cm^{-1} and 1589 cm^{-1} correspond to amide I (C=O stretching) and amide II (N–H bending) vibrations, respectively, confirming the successful deacetylation of chitin. The band observed near 1020 cm^{-1} is associated with C–O stretching vibrations of the polysaccharide backbone.

Upon incorporation of silica, noticeable changes occur in the FTIR spectra of the composite coatings. In all chitosan–silica samples, the appearance of a new absorption band at approximately 430–450 cm^{-1} is attributed to Si–O–Si stretching vibrations, confirming the successful incorporation of silica into the polymer matrix. In addition, the broad O–H/N–H stretching band shifts slightly toward lower wavenumbers and becomes broader with increasing silica content, indicating enhanced hydrogen bonding interactions between silanol (Si–OH) groups and the hydroxyl or amino groups of chitosan, thereby reflecting a stronger interfacial chemical association.

Notably, the BKS2 sample exhibits the most pronounced band broadening and peak shift in the O–H/N–H region compared to BK and other composite coatings. This behavior suggests an optimal level of interfacial interaction between chitosan chains and silica particles at 2% silica loading, leading to a more interconnected and stabilized hydrogen-bonded network within the matrix. Such interactions are expected to reduce free volume and microvoids within the coating, thereby resulting in a denser, more compact, and structurally integrated film that is capable of offering improved protective performance.

At higher silica contents (BKS3 and BKS4), no further significant shifts in the O–H/N–H stretching region are observed. Instead, the intensity of silica-related bands increases without evidence of stronger interfacial bonding. This suggests that excess silica may be less effectively integrated into the chitosan matrix, potentially leading to particle aggregation rather than uniform dispersion. Although direct microstructural evidence is required to confirm this effect, the FTIR results indicate that chemical interaction between chitosan and silica does not increase proportionally beyond 2% silica loading.

Overall, the FTIR analysis demonstrates that silica is successfully incorporated into the chitosan matrix and participates in hydrogen bonding interactions. The most effective interaction is observed at 2% silica loading, which correlates with the superior corrosion resistance observed in weight loss and EIS measurements. This confirms that chemical compatibility and interfacial bonding play a critical role in determining the protective performance of the chitosan–silica composite coatings.

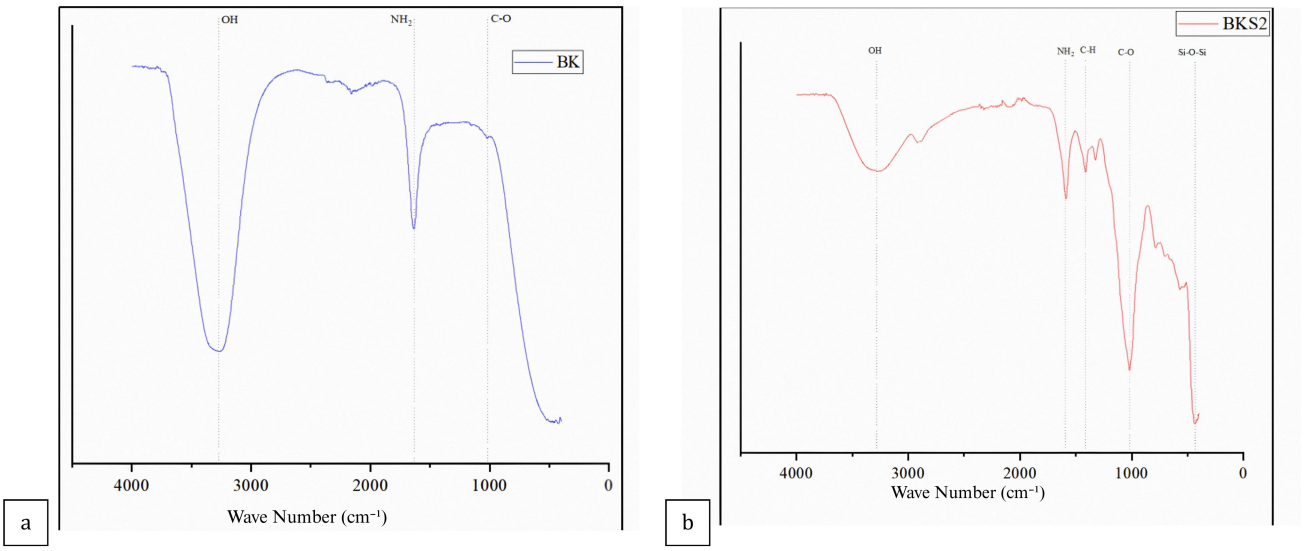

Figure 1. FTIR spectra of (a) Chitosan and (b) Chitosan–silica composite.

Table 3. Functional groups identified in chitosan and chitosan–silica composite.

Wave Number (cm⁻¹)	Functional Group	Chitosan	Chitosan-Silica Composite
3298.83 / 3269.05	O–H stretching	✓	✓
1637.29 / 1588.94	N–H (amine)	✓	✓
1413.76	C–H bending	–	✓
1019.74 / 1018.41	C–O stretching	✓	✓
433.36	Si–O–Si (siloxane)	–	✓

Corrosion Testing of Steel by Weight Change Method

The corrosion behavior of coated and uncoated ASTM A36 steel specimens was evaluated using the weight loss method after 7 days of immersion in a 10% NaCl solution. The initial and final masses, weight loss values, calculated corrosion rates, and coating efficiencies are presented in **Table 4**, while the corresponding trends are illustrated in **Figure 2**.

Uncoated steel (BB) exhibited the highest corrosion rate, confirming the severe corrosive nature of the chloride-rich environment. The application of a pure chitosan coating (BK) resulted in a slight reduction in corrosion rate compared to bare steel, indicating that chitosan acts as a physical barrier against the ingress of corrosive species and is capable of providing a modest level of protection to the underlying substrate.

A significant improvement in corrosion resistance was observed upon incorporation of silica into the chitosan matrix. Among all coating systems, the chitosan–silica composite containing 2% silica (BKS2) exhibited the lowest corrosion rate (0.0014 mm·y^{-1}) and the highest coating efficiency (89.67%). In contrast, coatings with higher silica contents (BKS3 and BKS4) showed increased corrosion rates, suggesting a decline in protective performance at excessive filler loadings.

These results indicate that an optimal silica content exists, at which the barrier properties of the chitosan coating are maximized, while excessive silica addition may adversely affect coating integrity.

Electrochemical Impedance Spectroscopy (EIS)

Electrochemical impedance spectroscopy (EIS) was employed to further evaluate the corrosion protection performance of the coatings in a 10% NaCl solution. Representative impedance spectra for uncoated steel (BB), chitosan-coated steel (BK), and chitosan–silica composite with 2% silica (BKS2) are shown in **Figure 3**.

The Nyquist plots exhibit capacitive semicircles, indicating that the corrosion process is predominantly controlled by charge transfer. The uncoated steel shows a small semicircle, reflecting low corrosion resistance. In contrast, the coated samples display significantly larger semicircles, indicating enhanced corrosion resistance due to the presence of the protective coating layer.

To quantitatively analyze the impedance response, the experimental data were fitted using appropriate equivalent electrical circuit models, as illustrated in **Figure 4**.

The fitted electrochemical parameters are summarized in **Table 5**. The BKS2 coating exhibits a markedly higher polarization resistance (Rp) value compared to BK and BB, indicating superior corrosion protection. This improvement is attributed to the incorporation of 2% silica, which enhances the barrier properties of the chitosan matrix by reducing coating permeability and inhibiting charge transfer at the steel–electrolyte interface. The lower CPE-P value observed for BKS2 suggests a more ideal capacitive behavior, which is associated with a denser and homogeneous protective layer.

Overall, the corrosion resistance follows the order BKS2 > BK > BB, which is in good agreement with the gravimetric corrosion (weight loss) results.

Table 4. Corrosion rate calculations for coated and uncoated steel specimens.

Sample Code	Initial Mass (g)	Final Mass (g)	Weight Loss (mg)	Corrosion Rate (mm·y⁻¹)	Average Corrosion Rate (mm·y⁻¹)	Efficiency (%)
BB (Blank)	4.27	4.98	7.1	0.0118	0.0136	0.00
	4.29	5.23	9.4	0.0156		
BK (Chitosan)	4.37	5.08	7.1	0.0117	0.0127	6.67
	4.40	5.23	8.3	0.0138		
BKS1 (Chitosan + 1% Silica)	4.36	4.57	2.1	0.0035	0.0036	73.33
	4.41	4.64	2.3	0.0038		
BKS2 (Chitosan + 2% Silica)	4.43	4.54	1.1	0.0018	0.0014	89.67
	4.45	4.51	0.6	0.0010		
BKS3 (Chitosan + 3% Silica)	4.48	4.73	2.5	0.0042	0.0044	67.87
	4.39	4.67	2.8	0.0046		
BKS4 (Chitosan + 4% Silica)	4.42	5.16	7.4	0.0123	0.0117	14.54
	4.38	5.05	6.7	0.0111		

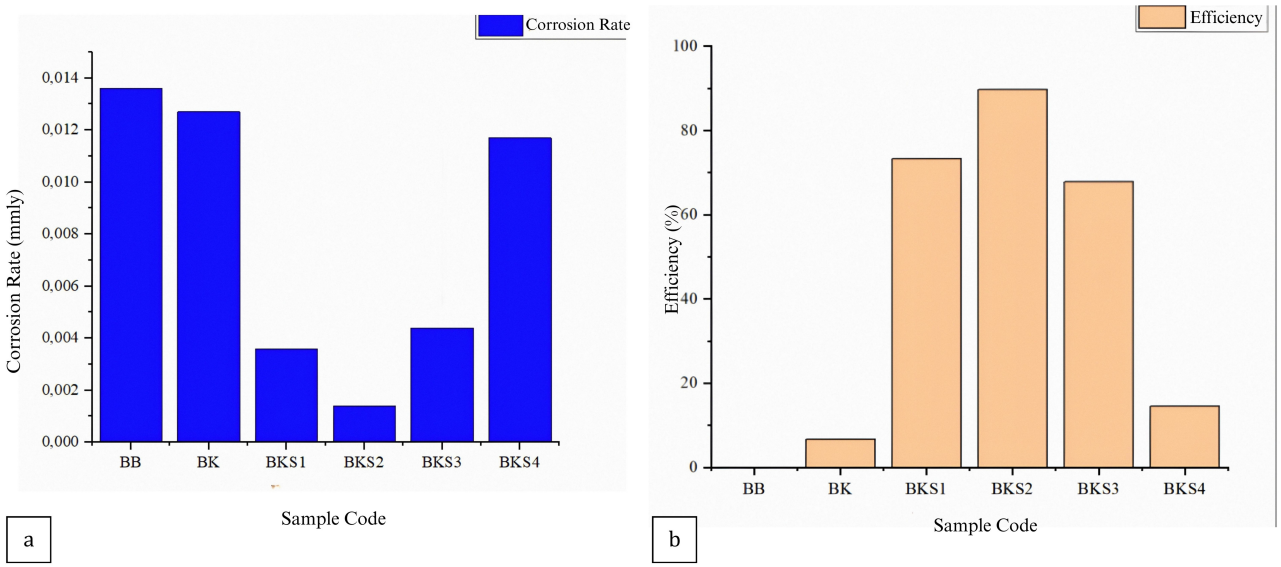

Figure 2. Graphs of (a) Corrosion rate and (b) Coating efficiency.

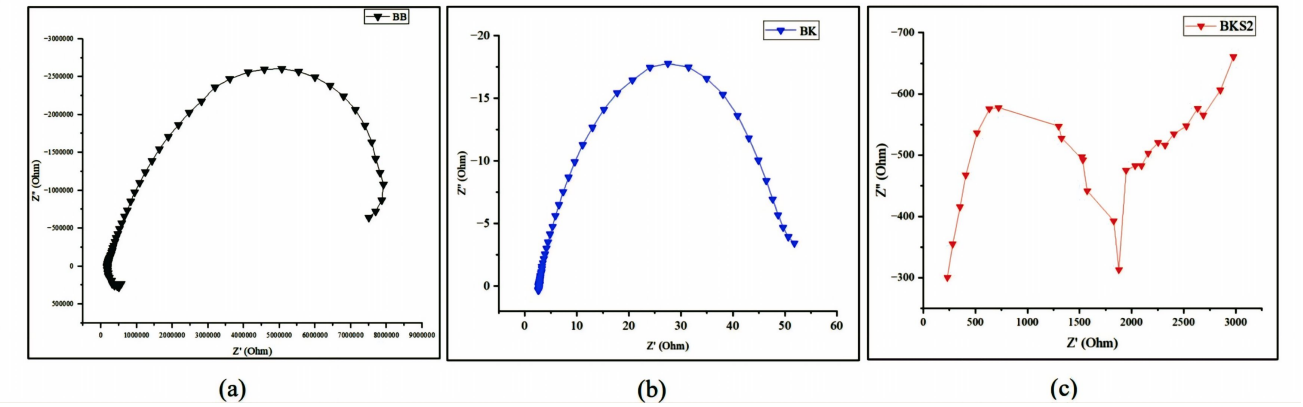

Figure 3. Nyquist plots of ASTM A36 steel: (a) Uncoated, (b) Chitosan-coated, and (c) Chitosan/silica composite (2%).

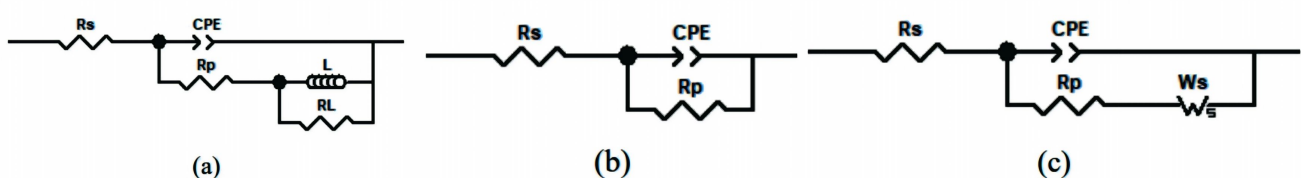

Figure 4. Equivalent electrical circuit models for (a) BB, (b) BK, and (c) BKS2.

Table 5. Electrochemical parameters of ASTM A36 steel with chitosan and chitosan–silica coatings.

Sample Code	Rp (Ω)	CPE-T	CPE-P
BB	21.75	0.00380	0.90429
BK	56.24	0.01060	0.73916
BKS2	2207	0.00002	0.65418

Note: The electrochemical parameters were obtained by fitting the EIS data using an Rs–(CPE‖Rp) equivalent circuit model. The corrosion resistance performance was primarily evaluated based on the polarization resistance (Rp), as this parameter directly represents the charge-transfer resistance at the steel–electrolyte interface.

Surface Examination of Steel

Surface morphology of selected ASTM A36 steel samples after 7 days of immersion in 10% NaCl solution was examined to visually assess the corrosion damage and coating protection. Representative surface images of uncoated steel (BB), chitosan-coated steel (BK), and chitosan–silica composite coating with 2% silica (BKS2) are presented in **Figure 5**.

The uncoated steel surface (BB) exhibits severe corrosion damage, characterized by extensive reddish-brown rust layers covering most of the surface, indicating aggressive corrosion in the chloride-rich environment. This observation is consistent with the high corrosion rate obtained from gravimetric measurements.

The chitosan-coated sample (BK) exhibits moderate corrosion, characterized by visible dark patches and partial rust formation. Although the chitosan coating provides a certain degree of barrier protection, localized corrosion is still evident, suggesting that the pure biopolymer coating has limited long-term effectiveness.

In contrast, the chitosan–silica composite coating containing 2% silica (BKS2) exhibits a relatively smooth and cleaner surface with minimal corrosion products. The reduced rust formation indicates improved coating integrity and enhanced resistance to chloride penetration. This improved surface condition is consistent with the significantly lower corrosion rate obtained from weight loss measurements and the higher polarization resistance observed in EIS analysis.

Overall, the surface examination confirms that the incorporation of an optimal amount of silica enhances the compactness and protective performance of the chitosan coating. The visual observations support the proposed corrosion protection mechanism derived from FTIR, gravimetric, and electrochemical analyses.

Discussion

Chitosan was successfully extracted from crab shell waste through sequential deproteinization, demineralization, and deacetylation processes, consistent with established procedures reported in the literature (13, 14). Crab shells were selected as the raw material due to their higher chitosan content compared to shrimp shells and fish scales, making them an efficient and sustainable source for biopolymer production (15). The extracted chitosan was subsequently dissolved in acetic acid to form a homogeneous coating solution, into which silica particles were incorporated at different loadings (1–4%) to modify the structural and protective properties of the coating.

FTIR analysis confirmed the characteristic functional groups of chitosan, including O–H, N–H, and C–O vibrations, indicating successful deacetylation and preservation of the polysaccharide backbone (16). In the chitosan–silica composites, the appearance of Si–O–Si stretching vibrations at approximately 433 cm^{-1} confirms the successful incorporation of silica into the polymer matrix, in agreement with previous studies (17). Additionally, subtle shifts and broadening of the O–H/N–H stretching region observed particularly in the BKS2 sample suggest enhanced hydrogen bonding interactions between chitosan chains and surface silanol groups. These interactions indicate improved interfacial compatibility, which is expected to reduce free volume and microvoids within the coating structure.

The corrosion performance evaluated by weight loss measurements reveals a strong dependence on silica loading. Uncoated steel exhibited severe corrosion, confirming the aggressive nature of the chloride-rich environment. The application of a pure chitosan coating resulted in only a modest reduction in corrosion rate, indicating that chitosan primarily acts as a physical barrier with limited resistance to long-term electrolyte penetration. In contrast, the incorporation of silica significantly improved corrosion resistance, with the BKS2 coating (2% silica) exhibiting the lowest corrosion rate and highest protection efficiency.

This enhanced performance can be attributed to the role of silica as a reinforcing filler within the chitosan matrix. At optimal loading, silica particles are likely to be well distributed, increasing coating compactness and creating a more tortuous diffusion pathway for chloride ions. This effectively delays electrolyte transport to the metal surface and suppresses corrosion reactions. However, at higher silica contents (BKS3 and BKS4), corrosion resistance decreased. Excessive filler loading may disrupt matrix continuity and promote structural defects or particle clustering, which can

Figure 5. Surface morphology of ASTM A36 steel after 7 days immersion in 10% NaCl solution: (a) BB (uncoated), (b) BK (chitosan-coated), and (c) BKS2 (chitosan–silica composite, 2%).

act as preferential pathways for electrolyte ingress. Although direct microstructural evidence is required to confirm this phenomenon, similar trends have been widely reported for polymer–inorganic composite coatings at high filler concentrations (18).

Electrochemical impedance spectroscopy further supports the gravimetric findings and provides insight into the corrosion protection mechanism. The Nyquist plot of uncoated steel exhibits a small semicircle, indicative of low charge-transfer resistance and rapid corrosion kinetics. The chitosan-coated sample shows an increased semicircle diameter, reflecting partial inhibition of charge transfer at the metal–solution interface. Notably, the BKS2 coating displays a substantially larger and depressed semicircle, characteristic of enhanced barrier properties and surface heterogeneity commonly associated with composite coatings (19). The significant increase in polarization resistance for BKS2 confirms that silica incorporation effectively suppresses electrochemical corrosion processes by limiting both ionic transport and interfacial charge transfer (20, 21).

The surface morphology observations are consistent with both gravimetric and electrochemical results. Severe rust formation on uncoated steel confirms uncontrolled corrosion, while the chitosan-coated surface shows partial protection with localized corrosion. In contrast, the BKS2-coated steel exhibits a smoother and cleaner surface with minimal corrosion products, indicating improved coating integrity and resistance to chloride penetration. This visual evidence supports the proposed mechanism in which optimized silica loading enhances coating compactness and durability.

Overall, the combined FTIR, weight loss, EIS, and surface examination results demonstrate that corrosion protection is governed not only by the presence of silica, but by its effective interaction and dispersion within the chitosan matrix. The optimal performance observed at 2% silica loading arises from synergistic effects between chitosan's film-forming capability and silica's reinforcing role, which together improve barrier properties, inhibit charge transfer, and reduce corrosion kinetics at the metal–solution interface.

Conclusion

This study confirms that chitosan–silica composite coatings improve the corrosion resistance of ASTM A36 steel in a chloride-rich environment. Among the investigated formulations, the coating containing 2% silica (BKS2) exhibited the most effective protection. This performance is attributed to optimal interfacial interactions between chitosan and silica, leading to a denser and more homogeneous coating structure that restricts the penetration of corrosive species and hinders charge transfer at the metal–electrolyte interface.

At higher silica loadings, the corrosion protection decreased, which is likely related to reduced coating uniformity and ineffective particle integration, potentially resulting in structural defects that facilitate electrolyte ingress. Although minor inconsistencies in gravimetric mass change and instability during EIS fitting were observed, the overall trends from FTIR, weight loss, electrochemical, and surface analyses consistently indicate the superior performance of the BKS2 coating.

These findings highlight the potential of chitosan–silica composites as environmentally friendly anticorrosion coatings, while also emphasizing the need for further optimization, long-term exposure studies, and improved electrochemical modeling to fully validate their practical applicability.

Declarations

Author Informations

Wardah Maulida Saldi
Affiliation: Department of Physics, Faculty of Science and Technology, State Islamic University of Maulana Malik Ibrahim Malang, Malang - 65145, Indonesia.
Contribution: Data Curation, Formal analysis, Visualization, Writing - Original Draft, Writing - Review & Editing.

Erna Hastuti ✉
Corresponding Author
Affiliation: Department of Physics, Faculty of Science and Technology, State Islamic University of Maulana Malik Ibrahim Malang, Malang - 65145, Indonesia.
Contribution: Conceptualization, Funding acquisition, Methodology, Project administration, Resources, Supervision, Validation, Writing - Review & Editing.

Acknowledgment
This study was motivated by ethical values emphasizing responsible use of knowledge, environmental stewardship, and sustainable utilization of natural resources. The use of crab shell waste as a chitosan source reflects an effort to add value to organic waste while addressing corrosion protection. The authors acknowledge the environmental risks associated with chemical-intensive extraction processes and encourage future research toward greener and more environmentally friendly coating technologies.

Conflict of Interest
The authors declare no conflicting interest.

Data Availability
The unpublished data is available upon request to the corresponding author.

Ethics Statement
Ethical approval was not required for this study.

Funding Information
The authors declare that no financial support was received for the research, authorship, and/or publication of this article.

References
1. Li X, Zhang X, Yan X, Zhang H. Corrosion behavior and mechanical properties of metallic materials. Materials. 2025;18(5):1009.

2. Zainal Arifin M, Kustono D. Characteristics of ASTM A36 steel plate corrosion rate due to bending treatment with angle, corrosion media, and corrosion time variations. J Eng Appl Technol. 2020;1(1):21–9.

3. Pratama RGP, Pratiwi DK, Utami NPE. The effect of time variation on corrosion behaviour of ASTM A36 in seawater from West Bangka of Bangka Belitung Islands, Indonesia. J Mech Sci Eng. 2022;8(2):19–23.

4. Wiradinata TA, Daryus A, Sugiyanto D, Nopryandi, Ikhsan M. Analysis of corrosion rate in low-carbon steel ASTM A36 and AISI 1020 in sulfuric acid solution using heat treatment temperature and immersion time variations. J Konversi Energi Manufaktur. 2025:44–52.

5. Iannuzzi M, Frankel GS. The carbon footprint of steel corrosion. NPJ Mater Degrad. 2022;6(1):101.

6. Aslani F, Dehestani M. Probabilistic impacts of corrosion on structural failure and performance limits of reinforced concrete beams. Constr Build Mater. 2020;265:120316.

7. Dalmora GPV, Borges Filho EP, Conterato AAM, Roso WS, Pereira CE, Dettmer A. Methods of corrosion prevention for steel in marine environments: A review. Results Surf Interfaces. 2025;18:100430.

8. Ahmed MA, Amin S, Mohamed AA. Current and emerging trends of inorganic, organic and eco-friendly corrosion inhibitors. RSC Adv. 2024;14(43):31877–920.

9. Hamza SF, Shahen S, Abdel Karim AM, El-Rashedy AA, Hyba AM. Eco-friendly corrosion inhibitor chitosan methionine for carbon steel in 1 M hydrochloric acid solution: Experimental and theoretical approach. Sci Rep. 2025;15(1):15924.

10. Fernández-Solis C, Keil P, Erbe A. Molybdate and phosphate cross-linked chitosan films for corrosion protection of hot-dip galvanized steel. ACS Omega. 2023;8(22):19613–24.

11. Bhat SI, Mobin M, Islam S, Zehra S, Shahid-ul-Islam. Recent advances in anticorrosive coatings based on sustainable polymers: Challenges and perspectives. Surf Coat Technol. 2024;480:130596.

12. Riahipour R, Nemati MS, Zadehmohamad M, Abadyan MR, Tehrani M, Baniassadi M. Mechanical properties of an epoxy-based coating reinforced with silica aerogel and ammonium polyphosphate additives. Polym Polym Compos. 2022;30:09673911211069019.

13. Tissera WMJCM, Rathnayake SI, Abeyrathne EDNS, Nam KC. Improved extraction and purification method for obtaining high-quality chitin and chitosan from blue swimmer (Portunus pelagicus) crab shell waste. Food Sci Biotechnol. 2021;30(13):1645–55.

14. Aberoumand A, Hoseinian M. Extraction of chitosan from shells of crab (Liocarcinus vernalis). Appl Food Res. 2025;5(1):100964.

15. Karim MM, Lasker T, Sahin MAZ, Hossain MS, Saputra HA. Low-cost production of chitosan biopolymer from seafood waste: Extraction and physiochemical characterization. J Res Updates Polym Sci. 2024;13:17–26.

16. Varma R, Vasudevan S. Extraction, characterization, and antimicrobial activity of chitosan from horse mussel Modiolus modiolus. ACS Omega. 2020;5(32):20224–30.

17. Susilowati E, Mahatmanti FW, Haryani S. Sintesis kitosan-silika bead sebagai pengadsorpsi ion logam Pb(II) pada limbah cair batik. Indones J Chem Sci. 2018;7(2):123-131.

18. Hattawi SN, Ahmed AG, Fadhil MF, Kuot SR, Alsubaie SM, Alazmi ML, et al. New approach for processing chitosan as low-cost protective hybrid coating for C-steel in acid media. Heliyon. 2024;10(13):e33743.

19. El-Shamy OAA, Deyab MA. Novel anticorrosive coatings based on nanocomposites of epoxy, chitosan, and silver. Mater Lett. 2023;330:133298.

20. Herrera Hernández H, Ruiz Reynoso AM, Trinidad González JC, González Morán OC, Miranda Hernández JG, Mandujano Ruiz A, et al. Electrochemical impedance spectroscopy (EIS): A review study of basic aspects of the corrosion mechanism applied to steels. In: Electrochemical Impedance Spectroscopy. IntechOpen; 2020.

21. Hussein MS, Fekry AM. Effect of fumed silica/chitosan/poly(vinylpyrrolidone) composite coating on the electrochemical corrosion resistance of Ti–6Al–4V alloy in artificial saliva solution. ACS Omega. 2019;4(1):73–8.

Additional Information

How to Cite
Wardah Maulida Saldi, Erna Hastuti. Eco-Friendly Chitosan–Silica Composite Coatings Derived from Crab Shell Waste for Enhanced Corrosion Protection of ASTM A36 Steel. *Aquatic Functional Products*. 2025;1(1):1-8

Publisher's Note
All claims expressed in this article are solely those of the authors and do not necessarily reflect the views of the publisher, the editors, or the reviewers. Any product that may be evaluated in this article, or claim made by its manufacturer, is not guaranteed or endorsed by the publisher. The publisher remains neutral with regard to jurisdictional claims in published maps and institutional affiliations.

Open Access